Electronic Supplementary Material (ESI) for Physical Chemistry Chemical Physics.

Electronic Supplementary information for

Static and Dynamic Electronic Characterization of Organic Monolayers Grafted on a Silicon Surface

O. Pluchery[a]*, Y. Zhang[b,c], R. Benbalagh[d], L. Caillard [a,e], J. J. Gallet[d], F. Bournel[d] A-F. Lamic-Humblot[f], M. Salmeron[b], Y. J. Chabal[e] and F. Rochet[d]

---

[a] *Sorbonne Universités, UPMC Univ Paris 06, CNRS-UMR 7588, Institut des NanoSciences de Paris, F-75005, Paris, France*

[b] *Materials Sciences Division, Lawrence Berkeley National Laboratory, Berkeley, CA 94720, USA.*

[c] *Applied Science and Technology Graduate Program, University of California at Berkeley, Berkeley, CA 94720, USA.*

[d] *Sorbonne Universités, UPMC Univ Paris 06, CNRS-UMR 7614, Laboratoire de Chimie Physique, Matière et Rayonnement, F-75005, Paris, France*

[e] *Laboratory for Surface and Nanostructure Modification, Department of Materials Science and Engineering, University of Texas at Dallas, 800 West Campbell Road, Dallas, Texas 75080, USA*

[f] *Sorbonne Universités, UPMC Univ Paris 06, CNRS-UMR 7197, Laboratoire de Réactivité de Surface, F-75005 Paris, France.*

1. Chemical preparation of the GOM

Grafted Organic Monolayers (GOMs) are highly ordered organic layers with a structural homogeneity that exhibit homogeneous electronic properties and a well-defined band structure. Compared to Self-Assembled Monolayers (SAMs) on metallic surfaces, GOMs are characterized by a covalent Si-C bond that ensures a strong chemical stability and the use of a semiconducting substrate offers the possibility of varying the doping level, which is the key for band engineering.

SiC_{11} and SiC_7 layers were grafted by thermal and UV-activated hydrosilylation, respectively. The first one, which relies on elevated temperatures to start the hydrosilylation reaction, has been extensively used and reported in the literature mainly because of its relative ease of use. Contrary to lots of other techniques, it does not require catalytic compounds that can oxidize and contaminate the surface.

UV activated hydrosilylation is slightly more complicated, involving the formation of a radical because the energy of the incoming light (~200-300nm so ~4-6eV) is higher than the energy of the Si-H bound (~3.5eV). The silyl radical created can then react with the alkene of the molecule inducing the formation of a Si-C bond. In contrast to thermal hydrosilylation, this technique allows the attachment of smaller molecules that would evaporate at temperatures needed for thermal hydrosililation. On the other hand, smaller molecules are prone to polymerization, so dilution, or introduction of inhibitors compounds is sometime needed. Chidsey *et al.* first reported the use of UV-initiated hydrosilylation to graft 1-pentene on a oxide free Si(111) surface in 1993.[1]

Samples of 8 × 10 mm^2 were cut from CZ n-doped silicon (111) (resistivity of 0.01 Ω·cm). Grafted organic monolayers were prepared within four steps (see Figure S1). In **step 1**, the samples were initially cleaned in a piranha solution at 80 °C (3:1 H_2SO_4 98%: H_2O_2 30%) then copiously rinsed with ultrapure water (18 MΩ·cm, Millipore). Atomically flat, hydrogen-terminated Si(111)-(1 × 1) surfaces were prepared by oxide removal in a concentrated HF solution for 30 sec, followed by a 150 sec immersion in 40% NH_4F solution followed by thorough rinsing in deionized water[9,5,132]. Caution is recommended because the piranha solution reacts strongly with organics, and the HF solution is extremely harmful. Both solutions should be handled with due protection: face shield, goggles, lab coat, apron and suitable gloves. Starting from a hydrogen-terminated Si(111)-(1 × 1) surface, step 2 consists of covalently attaching the organic layer by hydrosilylation with either a long alkyl chain of 11 carbon atoms (SiC_{11} samples) or a shorter chain with 7 carbon atoms (SiC_7 samples).

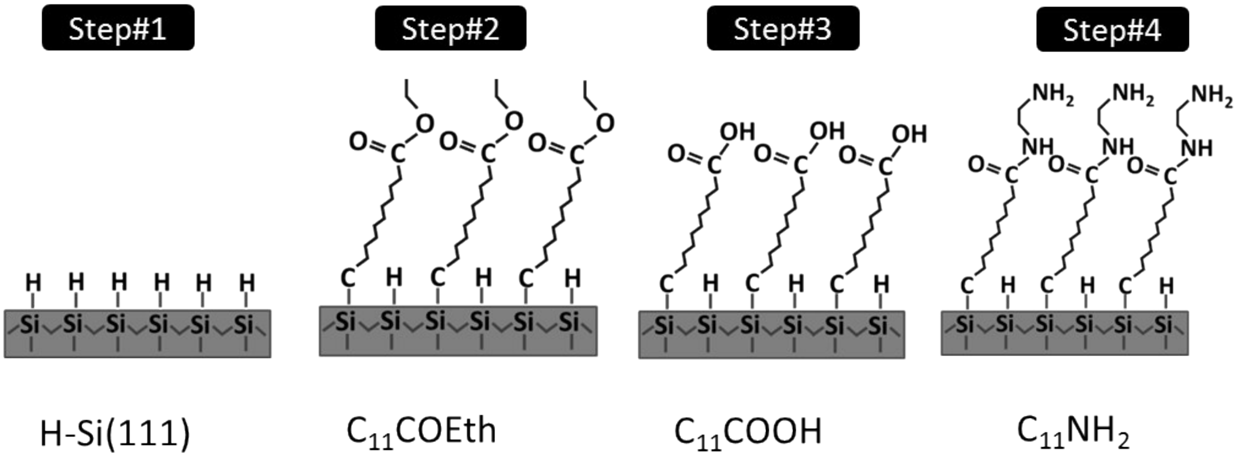

*Figure S 1***:** *The four steps for preparing the C_{11} grafted organic monolayers. Only C_{11}COEth and $C_{11}NH_2$ are considered in this study. C_{11}COOH is a step that we did not investigate with XPS. The different schemes for the C_7 alkyl chain are similar and are not represented here.*

SiC_{11}. 10-Carboxydecyl organic monolayers were grafted on the hydrogenated silicon via direct thermal hydrosilylation of ethyl undecylenate. The neat alkene was outgassed three times by freezing it using liquid nitrogen under low vacuum (10^{-2} Torr) in a Schlenk tube. It was then heated up to 200 °C under continuous argon bubbling when inserting the freshly prepared H-terminated silicon sample. Grafting was performed for 4 h.

SiC_7. 6-Carboxydecyl organic monolayers were grafted on the hydrogenated silicon via UV activation in a customized quartz cell where the sample was placed between two quartz slides. Notice that the molecule has a boiling point of 164.7°C and cannot be reacted at 200°C like C_{11}. All the steps are performed in a nitrogen-purged glove box (UNIlab Glovebox Workstation MBRAUN) with a O_2 and H_2O level lower than 0.1 ppm. It is then irradiated (with 253, 350 and 375 nm wavelengths) for 4h.

At the end of this second step both organic monolayers are terminated with a protected carboxylic acid. In **step 3**, the functionalized surfaces were sonicated in ethyl acetate and rinsed in boiling dichloromethane (40 °C). The carboxylic acids groups were then deprotected by using potassium tert-butoxide in DMSO (for 90 s and then rinsed thoroughly with DMSO) and by finally using an acid solution (HCl) to protonate the active group. Finally, **step 4** is the transformation of the functional headgroup into succinimidyl ester-terminated. This was performed by reaction with an aqueous solution of N-ethyl-N′-(3-(dimethylamino)propyl)-carbodiimide (EDC) and 2-morpholinoethanesulfonic acid (MES). After a few minutes in EDC solution, 1 mL of ethylenediamine is added to the solution for 1 h 30 min at room temperature. Finally, the surface was rinsed with ultrapure water. During the last step, one amine group of the ethylenediamine molecule ($H_2N-CH_2-CH_2-NH_2$) reacts with the activated ester, leading to the attachment of the molecule via an amide bond ($-(C=O)-NH-CH_2-CH_2-NH_2$). It is very unlikely that the ethylenediamine binds in a bridging configuration through its two amine ends because the molecule length (2.99 Å) is shorter than the typical distance between two COOH groups estimated from the Si−Si distance. Therefore, at the end of step 4, the resulting surface presents amine groups on top of the layer[24,133,17]. Notice that due to steric hindrance on the Si(111) surface, only one silicon out of two is linked to a molecule, the other silicon being passivated by hydrogen as shown on Figure S-1.

Silicon samples with these different organic functionalizations were prepared in Dallas and shipped to Paris under argon atmosphere and quickly installed in an UHV chamber for preservation.

2. Chemical preparation of the ascorbic AuNP

The method used to synthesize nanoparticles with ascorbic acid was first reported by Stathis et al. 1958[2] and revisited more recenlty.[3, 4] Typically, 200 µL of an aqueous solution of $HAuCl_4{:}3H_2O$ (10 g L^{-1} of gold) is added to 25 mL of water at around 0°C (ice-cooled) in a beaker. Then, 1.5 mL of a Na_2CO_3 solution (21.2 g L^{-1}) and 1 mL of an ascorbic acid solution (7 g L^{-1}) are added under vigorous stirring. The solution becomes instantaneously dark red.

3. STM image of the C_{11}-NH_2

A commercial Scanning Tunneling Microscope (STM VT-XA) from Omicron was used to check the quality of the GOM at Institut des NanoSciences de Paris.

STM images were recorded for the $SiC_{11}NH_2$ surface. They show an identical surface organization as the SiC_7NH_2 shown in the main text. Figure S2 shows this surface recorded at 100K. The profile Figure S2-b shows the typical circularly shaped bundles of 4nm (arrow) assigned to groups of molecules titled similarly relatively to the surface. This profile also shows holes 1.2 nm deep on the surface; they are area where the molecule probably did not react properly and where the surface is still hydrogenated. Such spots are probably starting points for silicon oxidation as discussed in the text. Images were processed with the freely available software WSxM.[5]

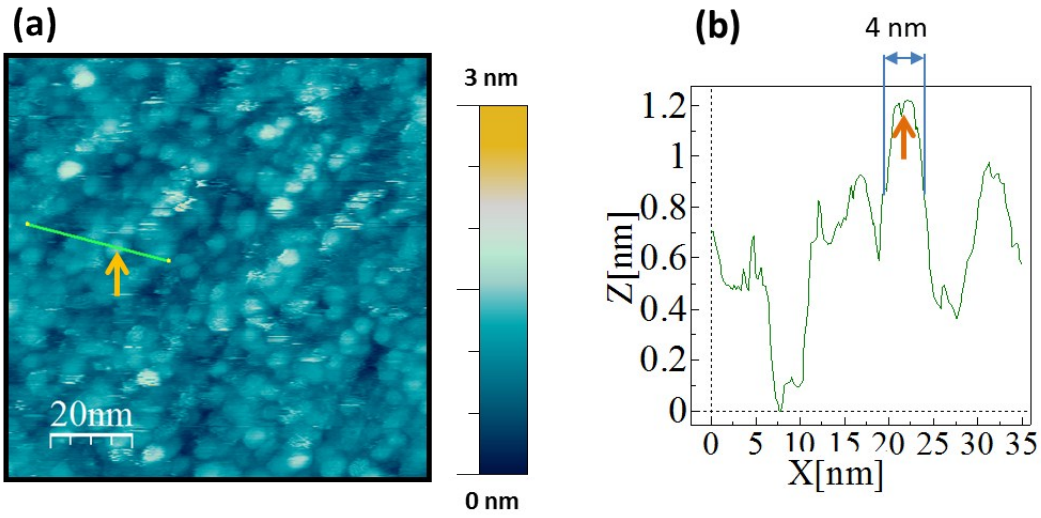

Figure S 2**:** (a) STM image (100x100nm) of the C7-NH_2 molecular layer grafted on Si(111) recorded at 100K under a bias of -2V. (b) Profile showing surface corrugation. A typical bundle of molecules is indicated with an arrow.

4. Surface sensitivity of our XPS characterization

Deconvolution of the XP spectra. X-Ray Photoelectron Spectroscopy (XPS) was carried out at Laboratoire de Chimie Physique Matière et Rayonnement in Paris, using a PHOIBOS 150 SPECS analyzer, operated in UHV conditions. The X-ray photoelectron spectra of Fig. 3 in the main text were deconvoluted into their main components. As the radiation is not monochromatized, the components have a winged shape that we account for using pseudo-Voigt curves (75% Gaussian and 25% Lorentzian), with a FWHM of 0.902 eV.[6] After a linear background subtraction, the Si $2p_{1/2}$ component around 99 eV was stripped from the Si 2p spectra using an iterative procedure, assuming a $2p_{3/2} – 2p_{1/2}$ spin orbit energy difference of 0.6 eV and a $2p_{1/2}$:$2p_{3/2}$ branching ratio of 0.5.[7, 8] This procedure eases the detection of surface components and oxidation states.

Surface sensitivity of XPS to chemical species. The intensity of the outermost Si layer (the one that bonds to the GOM) relative to the total core-level emission R_{111} was calculated by Himpsel *et al.* for Si(111) truncated between double layers (one broken bond) as:[8] $R_{111} = \left[1 - \exp\left(-\frac{4d_{111}}{\lambda}\right)\right] / \left[1 + \exp\left(-\frac{d_{111}}{\lambda}\right)\right]$, where $d_{111} = \frac{a\sqrt{3}}{12} = 0.0784\, nm$ (*a* is the silicon lattice parameter, 0.543 nm) and λ the inelastic mean free path in silicon, 1.6 nm at a photoelectron KE of ~1386 eV.[9] We find $R_{111} \sim 0.1$, *i.e.* the surface plane contributes to 10% of the total Si 2p peak intensity. The formula can also show that 90% of the Si 2p peak is obtained over a probing depth of 2λ=3.2 nm. Therefore we can conclude that *one atomic layer of a given species over our surface* contributes *to ~10% of the overall XPS signal, and 90% of the total signal is collected within the first 3.2 nm below the surface.*

Note that the highest surface sensitivity would be obtained at a KE around 30 eV, where λ is minimum: one Si surface plane would contribute to 40% of the total intensity.[8]

5. Band bending measurements via surface sensitive Si 2p core-level spectroscopy

We also use XPS to estimate the band bending qV_{bb}, by measuring the shift of the Si 2p. The accuracy of this estimation is clearly related to the surface sensitivity of the technique and it yields relevant values if the inelastic mean free path in silicon λ is sufficiently short compared to the thickness of the depletion layer where this band bending occurs. Indeed λ (1.6 nm at a photoelectron KE of ~1386 eV) is about one tenth of the depletion layer width (W =15 nm), calculated for the present wafers from the donor concentration ($N_D = 2\times10^{18}$ cm^{-3}).[10, 11]

The inelastic mean free path λ of the Si 2p photoelectron is 1.6 nm. This value must be compared to the width W of the depletion layer, on which a substantial band bending occur. When these values are comparable, we measure a value of qV_{bb} averaged over λ, that is $q\overline{V}_{bb}$.

$q\overline{V}_{bb}$ is calculated as follows. The electrostatic potential energy $q\varphi$ varies a function of x (the distance measured from the surface) according to the formula $q\varphi(x) = \frac{qV_{bb}}{W^2}(W-x)^2$, for $x<W$, while $q\varphi(x)=0$ for $x>W$ [10]

$q\overline{V}_{BB}$ is obtained by integration in the [0,W] interval:

$$q\overline{V}_{BB} = \frac{1}{\lambda}\int_0^W \frac{qV_{bb}}{W^2}(W-x)^2 e^{-\frac{x}{\lambda}}dx = qV_{BB}\left\{1-2\left(\frac{\lambda}{W}\right)+2\left(\frac{\lambda}{W}\right)^2\left(1-e^{-\frac{W}{\lambda}}\right)\right\} \qquad \text{Equation (1)}$$

For its part, W is calculated via the formula $W=\sqrt{\frac{2\varepsilon_0\varepsilon_r\left|V_{bb}/q\right|}{N_{D/A}}}$, Equation (2)

where ε_r is the relative permittivity of silicon (11.2), q the electron charge, and $N_{D/A}$ the donor/acceptor impurity density.[10] In the present case W= 150 Å and λ=16 Å. Therefore we have $q\overline{V}_{bb} \approx 0.8qV_{bb}$. In other words, the "true" qV_{bb} value is 11% larger than the measured values. We did not take into account this small correction in Table 1 of the main text.

6. XPS analysis of the supported gold nanoparticles

X-ray Photoelectron Spectra of the Au 4f core level for the $C_{11}NH_2$-AuNP sample were also recorded and provide insights on the supported gold nanoparticles. XP spectra are presented in Figure S3 together with that of bulk gold. The Au $4f_{7/2}$ BE of the AuNP is found (to a precision of 0.08 eV) at the same position as that of bulk gold (84.0 eV). There is an abundant literature on the dependence of the BE with the size of the gold cluster.[12-15] On weakly interaction substrates (*a*-C, SiO_2), on which the particle is assumed to be neutral, the BE of Au $4f_{7/2}$ core-level shows a significant *increase* with respect to the bulk value when the size of the gold particles diminishes below a certain level (expressed in Au surface density in Ref.[16], that is 10^{15} Au atoms/cm^2. In the present case, the size and density the AuNP (average diameter of 8.2 nm with a density of 7×10^9 NP/cm^2) corresponds to a coverage of 1.2×10^{14} Au atoms/cm^2, that falls below that limit. The shift to higher BE is generally attributed[12, 13, 17, 18], to a *final state effect*, i.e. the interaction of the photoelectron with the positively charged cluster (the core-hole is not immediately neutralized). For clusters electronically coupled with the substrate the core-hole lifetime is short and the reduction (increase) of the photoelectron KE (BE) negligible. On the other hand, shifts towards lower BE than that of the bulk value are also reported in the literature, e.g. by Boccia et al.[12]. This effect is interpreted as *an initial state effect*, i.e. the negative charging of the particle. According to Boccia et al. such an effect (-0.5 eV for a 0.8 nm NP size), disappears for NP particle diameters exceeding 2.5 nm. Our recent KPFM work shows that a 10 nm nanoparticle deposited on SiC_7NH_2 GOM accommodates five supplemental electrons.[18] Their size is considerably greater than the limit size observed by Boccia et al. Therefore the present XPS measurement does not invalidate the possibility that the NP are charged. Should they be neutral, the BE uncertainty of 0.08 eV points to core-hole lifetime below 10-15 s[17, 19].

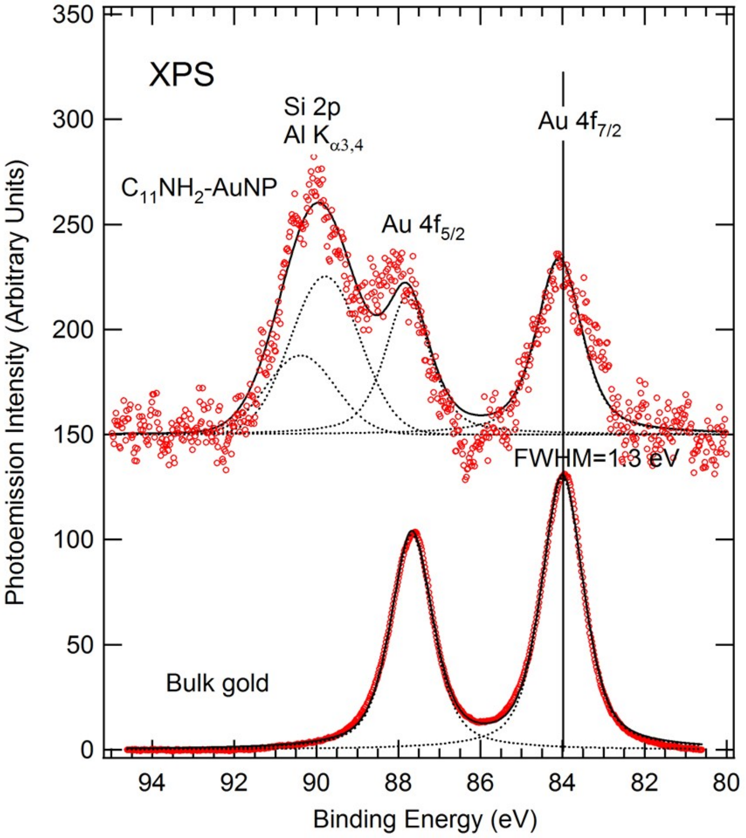

Figure S 3. XPS Au 4f core-level spectra of the $C_{11}NH_2$-AuNP Sample (top curve) and of bulk gold (red circles). The photon source is a non-monochromatized Al K_α anode. For the AuNP the Au $4f_{5/2}$ component merges with the Si 2p component of the substrate excited by the Al $K_{\alpha3,4}$ satellite of the main Al $K_{\alpha1,2}$ line. A fit (solid dark and dotted dark lines) of the C11-NH2-AuNP Sample is given (the Au 4f components are fitted with Voigt curves of FWHM=1.3 eV and a spin orbit splitting of 3.7 eV).

7. Secondary electron edge of all six samples.

WF is obtained from the secondary electron edge (SE) curve of the Ultraviolet Photoelectron spectra measured with the He source. To make sure that the SE electrons have a kinetic energy higher than the spectrometer vacuum level, the sample is negatively biased (V_{bias}~−20.14 V) with respect to the analyzer. V_{bias} is measured accurately (to 0.005 eV) from the BE shift of the Si 2p core-level spectra. The KE of the cutoff (KE_{cutoff}) is measured by extrapolating the edge of the peak to the zero baseline**.** The photon energy $h\nu$ is known (21.21 eV) and qV_{bias} is determined precisely by the increase in KE of the Si 2p core-level measured by XPS. The WF is calculated from: $WF = hv + KE_{cutoff} - (KE_{Fermi(unbiased)} + qV_{bias})$ where

$KE_{Fermi(unbiased)}$ is the kinetic energy of the Fermi level (measured on a clean gold surface) at qV_{bias}=0 eV.

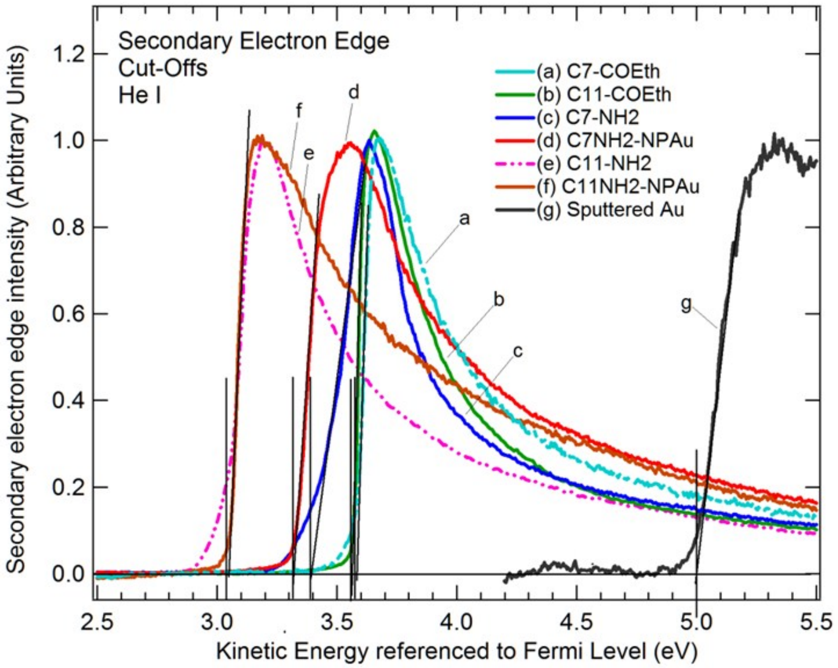

Figure S 4. Secondary electron edges measured with the He I lamp for the six different GOMs and for the sputtered gold foil. The cutoffs are indicated by the vertical bars. As the KE is referenced to the Fermi level, the cutoff KE is equal to the work functions of the different organic monolayers.

8. c-AFM image obtained at 0V bias

Conductive AFM was performed in a third UHV chamber (base pressure 5x10^{-9} torr) at Lawrence Berkeley National Laboratory and AFM images in contact mode were recorded on various places on the C_7-NH_2 surface and with various tip-sample bias. Below is an image recorded over an area of 400x200nm with the tip-sample bias set at 0V.

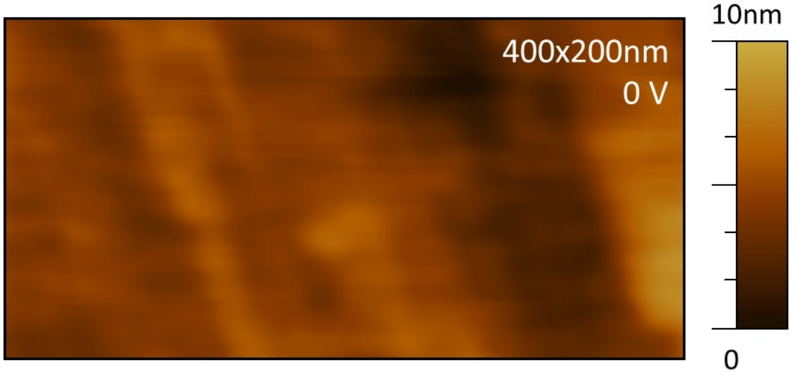

Figure S 4. AFM image in contact mode on the C_7-NH_2 sample. The image is taken with no applied bias and exhibits parallel stripes corresponding to the parallel terraces of the Si(111) samples due to a 0.5° miscut angle.

9. Plot of the band diagram

The representation of the band diagram of the AFM tip in contact with our insulating molecular layer grafted on silicon has been drawn by using the software designed by Knowlton and Southwick[20]. In drawing the energy profile, the dipole of the molecule was accounted for with 0.85 V shift in the applied bias.

We used the following parameters (Temperature *T* = 300K):

	Silicon (n-type)	GOM	AFM tip (Pt/Cr)
Thickness	50nm	1.3 nm	5 nm
Electron Affinity	4.05 eV	0.9 eV	
Work function			4.5 eV
Dopant	2E18 cm^{-3}		
Gap	1.17 eV	7.3 eV	
Dielectric constant	11.7	3.6	

References for the SI.

1. M. R. Linford, P. Fenter, P. M. Eisenberger and C. E. D. Chidsey, *J. Am. Chem. Soc.*, 1995, **117**, 3145-3155.
2. E. C. Stathis and A. Fabrikanos, *Chem. Ind.*, 1958, 860-861.

3. D. Andreescu, T. K. Sau and D. V. Goia, *J. Colloid & Interf. Sci.*, 2006, **298**, 742-751.
4. J. Han, F. Testard, F. Malloggi, P.-E. Coulon, N. Menguy and O. Spalla, *Langmuir*, 2012, **28**, 15966-15974.
5. I. Horcas, R. Fernandez, J. M. Gomez-Rodriguez, J. Colchero, J. Gomez-Herrero and A. M. Baro, *Rev. Sci. Instrum.*, 2007, **78**, 013705
6. G. Dufour, C. Poncey, F. Rochet, H. Roulet, M. Sacchi, M. De Santis and M. De Crescenzi, *Surf. Sci.*, 1994, **319**, 251-266.
7. F. J. Himpsel, B. S. Meyerson, F. R. M. Feely, J. F. Morar, A. Taleb-Ibrahimi and J. A. Yarmoff, School of Physics "Enrico Fermi", Varenna, 1988.
8. F. J. Himpsel, F. R. M. Feely, A. Taleb-Ibrahimi, J. A. Yarmoff and G. Hollinger, *Phys. Rev. B*, 1988, **38**, 6084-6096.
9. M. F. Hochella Jr and A. H. Carim, *Surf. Sci.*, 1988, **197**, L260-L268.
10. S. M. Sze, *Physics of Semiconductor Devices*, Second Edition edn., John Wiley & Sons, New-York, 1981.
11. R. G. Southwick and W. B. Knowlton, *Device and Materials Reliability, IEEE Transactions on*, 2006, **6**, 136-145.
12. A. Boccia, R. Zanoni, A. Arduini, L. Pescatori and A. Secchi, *J. Nanosci. Nanotechnol.*, 2012, **12**, 8851-8855.
13. A. Howard, D. N. S. Clark, C. E. J. Mitchell, R. G. Egdell and V. R. Dhanak, *Surf. Sci.*, 2002, **518**, 210-224.
14. H. Hövel, B. Grimm, M. Pollmann and B. Reihl, *Phys. Rev. Lett.*, 1998, **81**, 4608-4611.
15. M. G. Mason, *Phys. Rev. B*, 1983, **27**, 748-762.
16. J. J. Gallet, F. Bournel, F. Rochet, U. Köhler, S. Kubsky, M. G. Silly, F. Sirotti and D. Pierucci, *The Journal of Physical Chemistry C*, 2011, **115**, 7686-7693.
17. I. Magid, L. Burstein, O. Seitz, L. Segev, L. Kronik and Y. Rosenwaks, *J. Phys. Chem. C*, 2008, **112**, 7145-7150.
18. Y. Zhang, O. Pluchery, L. Caillard, A.-F. Lamic-Humblot, S. Casale, Y. J. Chabal and M. Salmeron, *Nano Letters*, 2015, **15**, 51-55.
19. D. C. Gleason-Rohrer, B. S. Brunschwig and N. S. Lewis, *The Journal of Physical Chemistry C*, 2013, **117**, 18031-18042.
20. B. Knowlton, http://nano.boisestate.edu/research-areas/multi-dielectric-energy-band-diagram-program/, 2006.